# Experimental and theoretical investigation of two- and threedimensional pressure waves propagating inside a tunnel due to a train passage

Peiffer A., Ottitsch F., Sockel H.
Institut für Strömungslehre und Wärmeübertragung
Technische Universität Wien, Wiedner Hauptstr. 7 A-1040 Wien

## Abstract

The problem of instantaneous threedimensional pressure waves inside of railway tunnels has been investigated theoretical and experimental. These waves do evolve whenever a pressure wave passes the train ends.

It is shown that such pressure waves can exist if the length of the passing wavefront is of the order of the tunneldiameter. They can either move in radial or tangential direction along the tunnel-axis. These higher mode waves travel slower than the primary wave thus introducing a dispersive effect. It is shown that in order to measure the radial moving waves a pressure transducer should be placed at the center of the cross–section of the tunnel. To measure waves moving in tangential direction the position for measurements should be the top of the tunnel ($\frac{\pi}{2}$) or ($\frac{\pi}{4}$) depending if single track or double track tunnels are to be investigated. For a tunnel of 14 m diameter the sampling frequency for such measurements should be about 160 Hz. The level of these higher mode waves can be of the order of the reflected wave.

The most important outcome of this work is, that such waves do neither transport mass nor momentum. Therefore such waves do not introduce an error in the common used one-dimensional theories.

## Nomenclature

### Latin Symbols

| | |
|---|---|
| $a_0^*$, $a^*$, $a$ | undisturbed speed of sound, speed of sound, dimensionless speed of sound |
| $a_{\varphi mn}$, $a_{gmn}$ | phase velocity, group velocity of mn-mode |
| $b$ | ratio of train radius to tunnel radius |
| $c_1$ | integration constant |
| $D_T$ | tunnel diameter |
| $f$, $g$ | seperation functions for $\Psi$ |
| $f_{mn}^{max}$ | maximum in the spectrum of time dependent transformation |

| | |
|---|---|
| $H$ | seperation functions for $\Phi$ |
| $L_T$ | tunnel length |
| $i$ | $\sqrt{-1}$ |
| $J_m$ | Bessel function of integer order m |
| $Mo$ | Measure for the strength of the higher mode waves |
| $k_{mn}$ | wave number |
| $m$, $n$ | index for eigenvalues in tangential and radial direction |
| $p^*$, $p_0^*$, $p$ | pressure, undisturbed pressure, dimensionless differential pressure |
| $p_f$, $p_{fc}$, $p_{ref}$ | filtered pressure, filtered pressure at center, reflected plane wave |
| $q_{mn}$ | $q_{mn} = \frac{\kappa_{mn}}{2\pi}$ |
| $r^*$, $r$ | coordinate in radial direction, dimensionless coordinate |
| $r_a$ | dimensionless radius of inlet tube |
| $S$ | dimensionless area of tunnel cross-section |
| $Sp$ | dimensionless area of idealized piston moving in tunnel |
| $t^*$, $t$ | time, dimensionless time |
| $t_1$ | dimensionless center of time for time dependent transformation |
| $u^*$, $u$ | fluid velocity in radial direction, dimensionless fluid velocity |
| $U_{mn}$, $V_{mn}$ | integration coefficients for $\Phi_{mnc}$ |
| $v^*$, $v$ | fluid velocity in tangential direction, dimensionless fluid velocity |
| $V_z^*$, $V_z$ | speed of train, dimensionless speed of train |
| $w^*$, $w$ | fluid velocity in axial direction, dimensionless fluid velocity |
| $w_f$ | window function for time dependent fourier transformation |
| $Y_m$ | Neumann function of integer order m |
| $z^*$, $z$ | coordinate in axial direction, dimensionless coordinate |

Greek Symbols

| | |
|---|---|
| $\epsilon_i$ | dimensionless length of wavefront |
| $\varphi$ | coordinate in tangential direction |
| $\Phi$ | velocity potential |
| $\Phi_{mnc}$ | coefficient of the infinite sum of the solution of $\Phi$ |
| $\Psi$ | seperation function for $\Phi$ |
| $\kappa_{mn}$, $\kappa$ | eigenvalue, isentropic exponent |
| $\Lambda_{mn}$ | orthonormalization coefficient |
| $\rho^*$, $\rho_0^*$, $\rho$ | density, undisturbed density, dimensionless density |
| $\tilde{*}$ | fouriertransformation of $*$ |
| $\breve{*}$ | timedependent-fouriertransformation of $*$ |
| $\hat{*}$ | othonormalized form of $*$ |
| $\omega$ | dimensionless frequency |
| $\langle\cdot\rangle$ | mean value of $\cdot$ per cross-section |

# 1 Introduction

One possible origin of discrepancies between measured and predicted pressure fluctuations in tunnels is, among other reasons, the way the train/tunnel system is represented.

The conventional method of calculating the flow around the train ends (see [6] or [7]) inside a tunnel is to assume infinitely thin, one–dimensional discontinuities. The idea behind this is, that the region of a three–dimensional flow is small compared to the train and tunnel length scales. While this approach seems - from the point of simplicity - very appealing, there remains the question in how far such a simplification is justified. Recent model- [8] and full–scale–experiments [9] showed that three–dimensional pressure waves do occur.

Due to this knowledge a research program has been started on the influence of three–dimensional flow regions inside of railway tunnels. In this paper attention is given to the developing three–dimensional flow due to the passing of a pressure wave over a train end.

Because of the difficulties, that arise with this problem, several simplifications for the theoretical considerations of the problem have to be made. We will focus our attention on the first order wave phenomenas.

As a further simplification we will regard the train speed to be small compared to the speed of sound, so that we can neglect it. This means, that the propagation of a pressure wave around the head of a train at rest in a tunnel is investigated.

The above simplifications are of course quite restrictive, but, as numerical simulations (which will be published in a Dissertation by Ottitsch, TU–Wien) have shown, it is still possible to get agreement between theory and experiments. We are quite confident, that this work offers a good model for the above described three–dimensional real flow. It helps to understand the advantages and disadvantages of the conventional method of calculating the flow around train ends.

# 2 Theoretical Considerations

## 2.1 Basic Equations

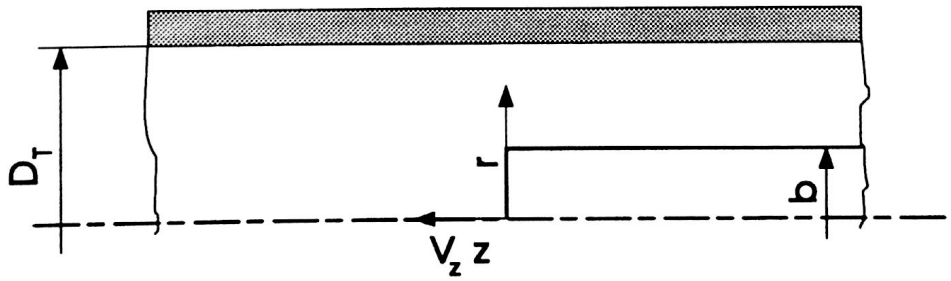


Figure 1: Geometry of problem

The present problem deals with the simulation of the fluid flow in the region of the train ends due to passing pressure waves. As our interest is focused on multidimensional pressure waves in the vicinity of train ends it seems quite obvious to neglect

heat and mass transfers along the side walls for such small scales. Furthermore as frictional losses are small over a scale of the tunnel length there is no need to include these effects in the current model. A fairly good approximation of the tunnel and train geometry is a semi–circular tube with a semi–circular cylinder (i. e. the train) moving inside (see fig. 1). This model allows rather simple analytical solutions, showing the principle properties of the developing three–dimensional waves. We would like to mention, that many concepts of the following work are to be found in [1].

We start our theoretical considerations assuming a compressible, isentropic, cylindrical flow with small pressure fluctuations. (In the following the asterix above a variable means, that this is a variable with a dimension. Whereas a variable without an asterix means, that this variable is dimensionless.) The coordinate-system is moving with $V_z$, the train speed. Thus we will get relative velocities. But, as long as the train speed is small compared with the speed of sound, we can neglect these differences for a first order calculation. By introducing the following dimensionless quantities

$$u = \frac{u^*}{a_0^*} \quad v = \frac{v^*}{a_0^*} \quad w = \frac{w^*}{a_0^*} \quad r = \frac{r^*}{D_T^*} \quad z = \frac{z^*}{D_T^*}$$
$$t = \frac{t^* a_0^*}{D_T^*} \quad V_z = \frac{V_z^*}{a_0^*} \quad p = \frac{p^* - p_0^*}{\rho_0^* a_0^{*2}} \quad \rho = \frac{\rho^*}{\rho_0^*} \quad a = \frac{a^*}{a_0^*}$$

it is possible to derive the dimensionless momentum- and continuity-equation like shown in [2].

$$\frac{\partial u}{\partial t} + u\frac{\partial u}{\partial r} + v\frac{\partial u}{r\partial \varphi} + (w + V_z)\frac{\partial u}{\partial z} - \frac{v^2}{r} = -\left(\frac{1}{1+\kappa p}\right)^{\frac{1}{\kappa}} \frac{\partial p}{\partial r} \tag{1}$$

$$\frac{\partial v}{\partial t} + u\frac{\partial v}{\partial r} + v\frac{\partial v}{r\partial \varphi} + (w + V_z)\frac{\partial v}{\partial z} + \frac{uv}{r} = -\left(\frac{1}{1+\kappa p}\right)^{\frac{1}{\kappa}} \frac{\partial p}{r\partial \varphi} \tag{2}$$

$$\frac{\partial w}{\partial t} + u\frac{\partial w}{\partial r} + v\frac{\partial w}{r\partial \varphi} + (w + V_z)\frac{\partial w}{\partial z} = -\left(\frac{1}{1+\kappa p}\right)^{\frac{1}{\kappa}} \frac{\partial p}{\partial z} \tag{3}$$

$$\frac{\partial p}{\partial t} = -u\frac{\partial p}{\partial r} - v\frac{\partial p}{r\partial \varphi} - w\frac{\partial p}{\partial z} - V_z\frac{\partial p}{\partial z} - (1+\kappa p)\left[\frac{\partial u}{\partial r} + \frac{\partial v}{r\partial \varphi} + \frac{\partial w}{\partial z} + \frac{u}{r}\right] \tag{4}$$

If one restricts these equations to small scales ($z$ of the order of several tunnel diameters) and to small disturbances ($V_z$ and $p \ll 1$) they can be linearized which yields:

$$\frac{\partial u}{\partial t} = -\frac{\partial p}{\partial r} \tag{5}$$

$$\frac{\partial v}{\partial t} = -\frac{\partial p}{r\partial \varphi} \tag{6}$$

$$\frac{\partial w}{\partial t} = -\frac{\partial p}{\partial z} \tag{7}$$

$$\frac{\partial p}{\partial t} = -\left(\frac{\partial u}{\partial r} + \frac{\partial v}{r\partial \varphi} + \frac{\partial w}{\partial z} + \frac{u}{r}\right) \tag{8}$$

For the two-dimensional case a simple finite difference method (i. e. McCormick-scheme see [2]) has been implemented which allows to solve the above equations numerically. In a Dissertation by Ottitsch (under preparation TU–Wien) the present theory is checked with such a numeric simulation. But this would go beyond the scope of the present paper. Here we just like to mention, that the numerical, theoretical and experimental results correspond well with each other. Thus one can be confident that the describred theory is valid for the considered problem.

## 2.2 Wave- and Helmholtz-equation

It is possible to simplify the above equations further. By introducing a potential $\Phi$

$$u = \frac{\partial \Phi}{\partial r} \quad v = \frac{\partial \Phi}{r\partial \varphi} \quad w = \frac{\partial \Phi}{\partial z} \quad p = -\frac{\partial \Phi}{\partial t}$$

the well known wave equation can be derived.

$$\frac{1}{r}\frac{\partial}{\partial r}\left(r\frac{\partial \Phi}{\partial r}\right) + \frac{\partial^2 \Phi}{r^2 \partial \varphi^2} + \frac{\partial^2 \Phi}{\partial z^2} - \frac{\partial^2 \Phi}{\partial t^2} = 0 \tag{9}$$

By means of the Fourier–transformation (and the inverse Fourier-transformation)

$$\tilde{\Phi}(\omega) = \tfrac{1}{2\pi}\int_{-\infty}^{\infty} \Phi(t)\, e^{i\omega t} dt \quad \Phi(t) = \int_{-\infty}^{\infty} \tilde{\Phi}(\omega)\, e^{-i\omega t} d\omega$$

and the seperation of variables

$$\Phi_{mn} = \Psi_{mn}(r, \varphi) * H_{mn}(z, t)$$

one gets from (9) periodic solutions for $\tilde{H}_{mn}$

$$\tilde{H}_{mn}(\omega, z) = e^{\pm iz\sqrt{\omega^2 - \kappa_{mn}^2}} = e^{\pm izk_{mn}} \tag{10}$$

and the Helmholtz-equation for $\Psi_{mn}$

$$\frac{1}{r}\frac{\partial}{\partial r}\left(r\frac{\partial \Psi_{mn}}{\partial r}\right) + \frac{\partial^2 \Psi_{mn}}{r^2 \partial \varphi^2} + \kappa_{mn}^2 \Psi_{mn} = 0 \tag{11}$$

with

$$\omega^2 = k_{mn}^2 + \kappa_{mn}^2 \tag{12}$$

Together with the boundary conditions for $\Psi_{mn}$ equation (11) leads to an Eigenvalue-problem. There is an infinite number of possible solutions with different $k_{mn}$ for each solution.

This shows, that, besides the plane fundamental wave propagating in the axial direction of a duct, there do exist waves which are reflected back and forward from the duct walls, as they propagate along the duct. These waves cause a nonuniform pressure distribution in a cross-section of the duct.

Equation (12) shows, that there exists a cutoff–frequency for each mode. In the power spectrum of a passing plane wave are certain driving frequencies. For driving frequencies above the cutoff–frequency a mode can be excited, propagating along the duct with almost no attenuation. For driving frequencies less than this $k_{mn}$ in equation (10) becomes complex and therefore $e^{\pm ik_{mn}z}$ leads to a strong attenuation. Such a mode cannot propagate as a wave.

## 2.3 Solution for a semi-circular duct

The above equations have to be solved for a duct with a semicircular cross-section. In a duct with rigid walls, the fluid velocity normal to the surface must be zero, which gives the following boundary-conditions:

$$\frac{\partial\Psi(r=0.5)}{\partial r} = 0 \quad \lim_{r\to 0}\left(\frac{\partial\Psi}{\partial r}\sin\varphi + \frac{\partial\Psi}{r\partial\varphi}\cos\varphi\right) = 0 \quad \frac{\partial\Psi(\varphi=0)}{r\partial\varphi} = 0 \; \frac{\partial\Psi(\varphi=\pi)}{r\partial\varphi} = 0$$

This boundary conditions have to be applied if there is no train in the tunnel. In the other case, where there is a train in the tunnel, the condition for $\Psi$ in the middle of the cross-section has to be changed to:

$$\frac{\partial\Psi(r=b)}{\partial r} = 0$$

With the separation of variables $\Psi_{mn} = f_{mn}(r) * g_m(\varphi)$ the solutions are:

$$f_{mn}(r) = [J_m(\kappa_{mn}r) + c_1 Y_m(\kappa_{mn}r)] \tag{13}$$

$$g_m(\varphi) = \cos m\varphi \tag{14}$$

Where $J_m$ and $Y_m$ are the Bessel- and Neumann–function of integer order $m$ respectively. For the empty tunnel $c_1 = 0$ and in the other case, where there is a train of radius $b$ inside the tunnel, $c_1$ is calculated by:

$$c_1 = -\frac{J'_m(\kappa_{mn}b)}{Y'_m(\kappa_{mn}b)}$$

The above functions form an orthogonal function system. The solution of equation (9) is calculated by adding up all single solutions and doing an inverse Fourier transformation:

$$\Phi = \sum_{m,\ n=0}^{\infty} \Phi_{mnc} = \sum_{m,\ n=0}^{\infty} \int_{-\infty}^{\infty} U_{mn} V_{mn}(\omega) * \hat{\Psi}_{mn} e^{i(k_{mn} z - \omega t)} d\omega \tag{15}$$

$\hat{\Psi}_{mn}$ is the orthonormalized form of $\Psi_{mn}$:

$$\hat{\Psi}_{mn} = \frac{1}{S\Lambda_{mn}} \Psi_{mn} \tag{16}$$

with for $m > 0$

$$\iint_S \Psi_{mn}^2 dS = \Lambda_{mn} S = \frac{1^2 \pi}{4} \left[ \left( 1^2 - \frac{m^2}{\kappa_{mn}^2} \right) f_{mn}^2(\kappa_{mn}) - \left( b^2 - \frac{m^2}{\kappa_{mn}^2} \right) f_{mn}^2(\kappa_{mn} b) \right] \tag{17}$$

and for $m = 0$

$$\iint_S \Psi_{0n}^2 dS = \Lambda_{0n} S = \frac{1^2 \pi}{2} \left[ f_{0n}^2(\kappa_{0n}) - b^2 f_{0n}^2(\kappa_{0n} b) \right] \tag{18}$$

The coefficients $U_{mn}$ represent the boundary conditions (without the frequency dependent part) and $V_{mn}$ follow from the initial conditions and the frequency dependent part of the boundary conditions. The analytic calculation of these coefficients is a quite complicated problem. In the following we will only need the assumption that $V_{mn}$ changes smoothly above the cuttoff-frequency of a given mode.

### 2.3.1 Empty tunnel

For the empty tunnel the values of $\kappa_{mn} = 2\pi q_{mn}$ follow from the boundary conditions:

$$\pi q_{mn} f_{m-1}(\pi q_{mn}) = m f_m(\pi q_{mn}) \tag{19}$$

Some values of $q_{mn}$ are listed in the following table:

| m | n=0 | n=1 | n=2 | n=3 |
|---|---|---|---|---|
| 0 | 0.0 | 1.2197 | 2.2331 | 3.2372 |
| 1 | 0.5861 | 1.6970 | 2.7140 | 3.7274 |
| 2 | 0.9722 | 2.1346 | 3.1734 | 4.1921 |
| 3 | 1.3369 | 2.5528 | 3.6128 | 4.6441 |
| 4 | 1.7 | 2.9 | | |
| 5 | 2.0 | | | |
| 6 | 2.38 | | | |

As expected, the fundamental mode (0, 0) has a zero characteristic value and thus is a plane wave. The cutoff frequency for the $(m, n)$-th mode is $q_{mn}$. Thus the first modes to become propagational are (1, 0), then (2, 0) both of which are waves which move in a spiral path and only after these two tangential modes the first radial mode (0, 1) starts to propagate.

### 2.3.2 Tunnel with train

In the case, where a train is inside the tunnel, the boundary conditions give the following equation for the Eigenvalues $q_{mn}$:

$$J'_m(\pi q_{mn})\, Y'_m(\pi q_{mn} b) - Y'_m(\pi q_{mn})\, J'_m(\pi q_{mn} b) = 0 \tag{20}$$

$b$ is the ratio between train and tunnel radius. In the following table the first few radial modes are listed for three different values of $b$. $b = 0.333$ is the value which would be appropriate for a modern german-train-tunnel configuration.

| b | n | $q_{0n}$ | b | n | $q_{0n}$ | b | n | $q_{0n}$ |
|---|---|---|---|---|---|---|---|---|
| | 1 | 1.326 | | 1 | 1.562 | | 1 | 3.515 |
| 0.181 | 2 | 2.512 | 0.333 | 2 | 3.036 | 0.714 | 2 | 7.008 |
| | 3 | 3.714 | | 3 | 4.525 | | 3 | 10.505 |
| | 4 | 4.924 | | 4 | 6.019 | | 4 | 14.004 |

## 2.4 Dispersion of the higher modes

The phase velocity of the mn-th mode is:

$$a_{\varphi mn} = \frac{\omega}{k_{mn}} = \frac{1}{\sqrt{1 - \left(\frac{\kappa_{mn}}{\omega}\right)^2}} \tag{21}$$

and the group velocity $a_{gmn}$ is:

$$a_{gmn} = \left(\frac{\partial k_{mn}}{\partial \omega}\right)^{-1} = \sqrt{1 - \left(\frac{\kappa_{mn}}{\omega}\right)^2} = \frac{1}{a_{\varphi mn}} \tag{22}$$

Below the cutoff–frequency the phase and the group velocities are imaginary, which means that such a wave cannot propagate. Slightly above the cutoff–frequency the phase velocity is large and real (the group velocity is small), and as $\omega$ approaches infinity $a_\varphi$ approaches 1 from above and $a_g$ approaches 1 from below. A mode, that is excited in the range of the cutoff–frequency, moves only slowly along the tunnel axis. Just the highfrequency components of the mode propagate with approximately the speed of the wave front of the signal. This means that the maximum of each mode in the frequency domain will move to higher frequencies as the wave travels along the duct as will be shown in the next section.

## 2.5 Timedependent-Fourier-Transform

The pressure field, that develops after a compression-wave has passed a train in a tunnel, consists of the primary wave and the higher modes, which propagate inside the tunnel. To analyze such an instantaneous, dispersive signal it is necessary to introduce the Timedependent-Fourier-Transform

$$\breve{f}(t_1, \omega) = \frac{1}{2\pi} \int_{-\infty}^{\infty} f(t)\, w_f(t - t_1) \exp(i\omega t) dt \tag{23}$$

If one uses this transformation for each coefficient $\Phi_{mnc}$ of equation (15) it is possible to show how the maxima in the frequency spectrum of each mode move to higher frequencies along the tunnel-axis.

The transformation of the coefficient $\Phi_{mnc}$ in equation (15) yields:

$$\breve{\Phi}_{mnc}(t_1, \omega) = \hat{\Psi}_{mn} U_{mn} \frac{1}{2\pi} \int_{-\infty}^{\infty} \int_{-\infty}^{\infty} V_{mn}(\omega')\, e^{i(k_{mn}(\omega')z - \omega' t)} d\omega' w_f(t - t_1)\, e^{i\omega t} dt \tag{24}$$

and after integration over $t$:

$$\breve{\Phi}_{mnc}(t_1, \omega) = \hat{\Psi}_{mn} U_{mn} \int_{-\infty}^{\infty} \tilde{w}_f(\omega - \omega')\, e^{ik_{mn}(\omega')z} e^{i(\omega - \omega')t_1} V_{mn}(\omega')\, d\omega' \tag{25}$$

where $\tilde{w}_f$ is the fourier transform of the window function $w_f$. By choosing the window function $w_f$ as a smooth, symmetric function which spreads out over a large time period and has its maximum at $w_f(0)$ one gets only a poor resolution in the transformed time-domain, but a rather good resolution in the transformed frequency-domain. This of course means that $\tilde{w}_f$ vanishes outside the region $\omega' = \omega$, which permits us to concentrate on this region when evaluating equation (25).

This assumption allows the use of a first order expansion for $k_{mn}(\omega')$ in equation (25):

$$k_{mn}(\omega') = k_{mn}(\omega) + \frac{\omega' - \omega}{\sqrt{1 - \left(\frac{\kappa_{mn}}{\omega}\right)^2}} \tag{26}$$

If the initial $V_{mn}(\omega')$ changes only slowly in the region of $\omega$, which means that $V_{mn}$ has no dominant periodic parts in the time domain, we get from equation (25):

$$\breve{\Phi}_{mnc}(t_1, \omega) = \hat{\Psi}_{mn} U_{mn} V_{mn}(\omega)\, e^{ik_{mn}(\omega)z} w_f\left(t_1 - \frac{z}{a_{gmn}}\right) \tag{27}$$

If we now further assume, that the coefficient $V_{mn}$, which describes the excitation of the mode-mn, behaves smooth above the cutoff–frequency, then equation (27) shows that the frequency $f_{mn}^{max}$ where each mode has its maximum is a function of $z$ (the distance from the train end) and $t_1$ (the region of the transformation).

$$2\pi f_{mn}^{max} = \omega_{mn}^{max} = \frac{\kappa_{mn}}{\sqrt{1-\left(\frac{z}{l_1}\right)^2}} \tag{28}$$

Therefore it is possible to distinguish between frequencies, that occur due to the three-dimensionality of the flow (these frequencies change with the distance from the train ends) and frequencies, which occur due to the experimental setup. Each local maxima in the frequency domain can be related to a single mode $\kappa_{mn}$.

## 2.6 The number $Mo$ as a measure for higher mode waves

As has been shown in the above sections the higher mode waves cannot exist beyond a certain cutoff–frequency. Therefore it seems to be obvious to filter a measured signal with a lowpass filter whose cutoff–frequency is substantially beyond the cutoff–frequency of the first mode and then substract this signal from the original signal. This new signal $p_f$ will represent the higher modes outside the region of the wave front. As most of the higher modes will stay beyond (see section 2.5) the front, it should be possible to analyze the higher modes with this method.

The reason why this method and not a highpass–filter was chosen is, that with this method an overshooting of the digital filter could be seen easily.

In the experiments a lowpass–Butterworth–filter of order ten and a cutoff–frequency of 75 % of the cuttoff–frequency of the first radial mode has been used.

A good measure for the degree of three–dimensionality is the time–averaged squared pressure signal averaged over the cross-section. Therefore the ratio between this value and the squared value of the pressure of the reflected one-dimensional wave $p_{ref}$ has been defined. In the following the brackets $\langle\cdot\rangle$ means, that it is the mean value over the cross-section.

$$Mo = \sqrt{\frac{\overline{\langle p_f^2 \rangle}}{p_{ref}^2}} \tag{29}$$

It can be shown (see [4]) that under the assumption, that the tangential modes are small, it is mainly the first radial mode which contributes to this value. (If the maxima in the power spectrum of the second radial mode is 20 % of the maxima of the first radial mode, then this mode contributes only 2.2 % to the value of $Mo$.) For this first radial mode the ratio of $\overline{\langle p_f^2 \rangle}$ and the corresponding mean value measured in the centre $\overline{p_{fc}^2}$ is $\Lambda_{01}$ as shown in [4]. Neglecting higher mode terms we can write:

$$Mo = \sqrt{\frac{\Lambda_{01}\overline{p_{fc}^2}}{p_{ref}^2}} \tag{30}$$

The above assumption has been justified by spectral analysis of the measured signals. The above equation (30) can be evaluated by calculating the standard

deviation of a filtered measured signal. The height of the reflected pressure wave $p_{ref}$ can be calculated using the mean value of the oncoming wave and the usual one-dimensional reflection coefficients.

A value of $Mo = 0.2$ could thus be interpreted in the way, that there are pressure fluctuations of approximately 20 % superimposed on the plane reflected wave.

In the following section all experiments have been compared with each other with this measure.

# 3 Model experiments

To check the validity of the above theory model experiments have been carried out. In these experiments the pressure transients inside a model tunnel where measured simultaneously at up to eight different points. The whole experimental setup is described in detail in [4] and a Dissertation by Ottitsch (to be published TU–Wien).

## 3.1 Experimental apparatus

In [5] Pope presents a good review of the various methods for the reduced scale modelling of the flow in tunnels. It seems that the majority of the reduced scale facilities have focused their attention on the global flow inside the tunnel model. To achieve this goal much emphasize has been given to the problem of how to move the trains inside the tunnel. But, to the knowledge of the author, there has only been a minor interest on local effects. With regrad to localized effects the Reynolds number and the Mach number of the models are not so important. There is less need to model closely the speed of the train, which greatly simplifies the construction of such a test facility.

But when investigating local effects some attention must be given to the fact that the study of localized flows need high sampling rates for the data acquisition. Thus it is the maximum achievable sampling rate which gives a minimum for the scale of the test facility. Due to the instrumentation at our institute (see 3.2) we have chosen a tunnel diameter of 0.21 m, which correspondends to a full scale diameter of 15.1 m for a scale of 1:72.

The principal setup of the experimental apparatus can be seen in figure 2. A pressure wave generator produces a pressure wave, which propagates along the first tube. At point 1 this wave is divided into two waves of equal intensities propagating through the second tube (see 3.3 for an explanation). At point 2 these pressure waves enter the tunnel simultaneously, so that an almost plane wave starts propagating in the tunnel section. The reason for this special arrangement is discussed in section 3.3.

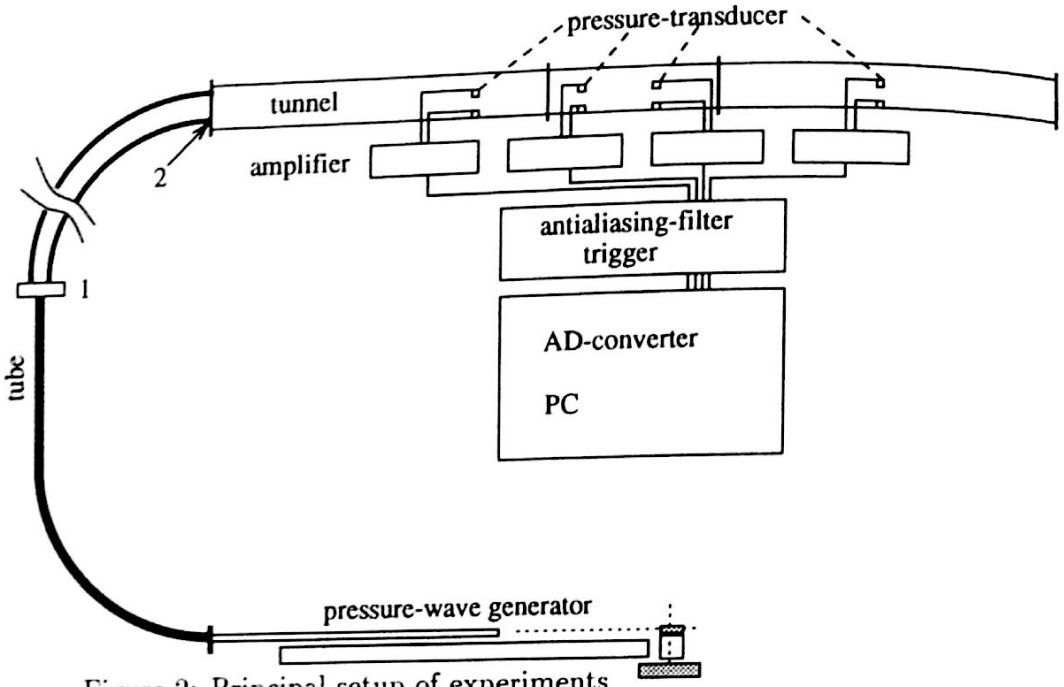


Figure 2: Principal setup of experiments

### 3.1.1 The pressure wave generator

The institute has a facility for generating pressure waves (see figure 3). A cable is accelerated very rapidly by means of an electric motor in connection with an electromagnetic clutch-brake system to constant speed. A catch fixed on the cable drives a bolt which impacts a very light piston, that is accelerated nearly instantaneously.

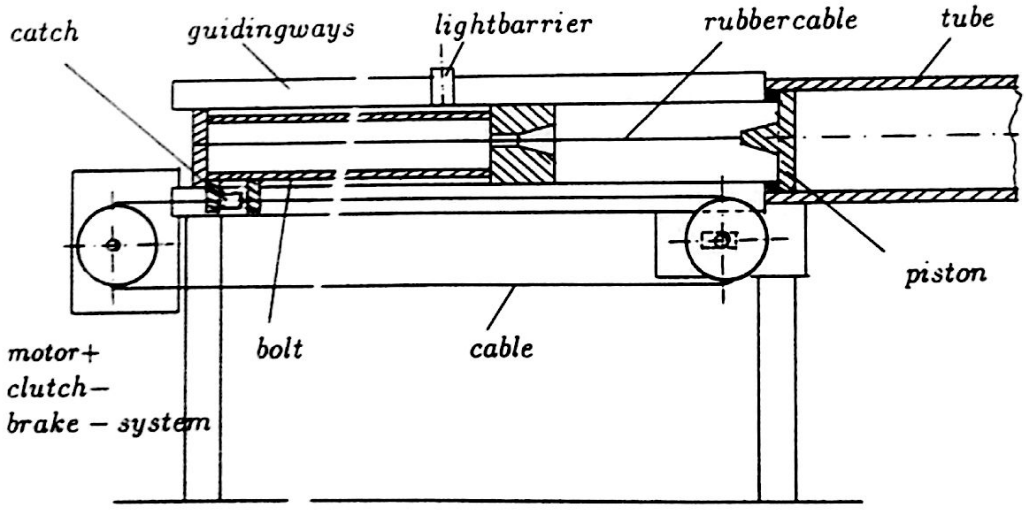


Figure 3: Pressure wave generator

This causes a pressure wave propagating inside the small tube (see figure 2). When the bolt passes a lightbarrier the clutch-brake system stops the bolt. Depending on the size of the driving wheel for the cable and the speed of the motor it is possible to get differential pressure waves between 0 - 1400 Pa in the tunnel section.

### 3.1.2 The tunnel model

The tunnel model has a diameter of 0.21 m and a length of 7.5 m. It has been made of 2 mm thick metal sheet. The cross–section has the shape of a semicircle. The bottom is made out of two 20 mm thick coated chip boards. The tunnel model does not take account of the ballasted track, which is to be found in most modern tunnels. It is known (see [3]) that such a ballasted track affects the shape of the propagating pressure waves. But, as the primary goal of the experiments is the understanding of multidimensional pressure waves, there was no need to model the track. During operation it turned out, that the tunnel section was not tight. Therefore a special packing rubber band had to be used for the sealing between the metal sheet and the chip board. Oscillations of the metal sheet were detected with accelerometers even before a pressure wave passed a measuring point. The effect of these oscillations was neglected. According to section 2.3.1 the cutoff–frequencies for the first two tangential and the first two radial modes are 957 Hz, 1588 Hz, 1992 Hz and 3647 Hz respectively.

### 3.1.3 The train models

The train models are made out plexiglass–tubes that were cut in half. The bottom is made of a plexiglass–plate. The length of the train models is 4 m. Three different diameters (38 mm, 70 mm and 150 mm) were chosen for the trains. During the experiments it turned out, that the shape of the pressure wave, which propagated along the train, changed, caused by the vibrations of the plexiglass-plates. To minimize this effect all train models were filled with gypsum. However, it is interesting to note, that this effect does happen and that it leads to an one–dimensional distortion of the pressure wave. In reality similar effects will occur due to vibrations of the train walls and mass transport in the train. Therefore it is recommended that an investigation of the change of the shape of a pressure wave propagating between a train and the tunnel wall should be undertaken. For the train model with a diameter of 70 mm a train nose was made out of PVC whose cross–sectional shape was similar to the shape of an ICE train nose. To get an estimate, in how far the real geometric boundary conditions have an influence on the problem, a quadratic beam (60 mm) made of wood was also investigated.

## 3.2 The instrumentation

For all measurements Kulite XCW-093 pressure transducers were used. These transducers have eigenfrequencies of about 100 kHz. Special differential amplifiers have been built at the institute with an amplifying factor of 400 and an offset correction. The output signal of these amplifiers was passed through an analog-filter whose cutoff-frequency could be adjusted to ensure a propper nyquist frequency for the AD-sampling. For the AD-sampling a DT-2821-F-8 DI card was used together with the software package Global Lab by Data-Translation. With this AD-card a continuous sampling rate of 130 kHz can be achieved on up to 8 channels. Thus each channel could be sampled with at least 16.25 kHz. Every channel has an accuracy of 12 bit. To minimize drift effects the whole instrumentation was powered on at least a night before an experiment. Usually it was not powered off for several days. Before each experiment the offset was corrected by a calibration.

With this instrumentation it is possible to analyze pressure waves down to 5 Pa in the time-domain. The noise level had a standard deviation of approximately 2 Pa. In the frequency domain pressure frequencies as little as 0.5 Pa could be distinguished.

## 3.3 The tunnel inlet section

We started our experiments with a test setup with only one tube connecting the pressure generator and the model tunnel (compare figure 2). At point 2 multi-dimensional pressure waves do evolve due to the big change in the cross-sectional area. The amplitudes of these pressure waves will certainly be much higher than those which evolve due to the relatively moderate change in cross-section caused by a train. Therefore we changed this first arrangement according to the results of the following theoretical considerations.

By assuming that the small inlet tube at the entrance has an effect similar to a piston moving with a frequency $\omega$, it can be shown [1] that the coefficients $U_{mn}$ in equation (15) for such a piston can be calculated by an integration over the area of the piston. If one evaluates this for a circular piston of radius $r_a$ moving inside a semi-circular cross-section and assumes, that the initial distribution $\Psi_0$ is constant over the cross-section of the piston one gets:

$$U_{mn} = \frac{1}{S\Lambda_{mn}} \iint_{Sp} \Psi_0 \Psi_{mn} r dr d\varphi = \frac{1}{S\Lambda_{mn}} \int_{x-r_a}^{x+r_a} \int_{\varphi_0-\varphi(r)}^{\varphi_0+\varphi(r)} \Psi_{mn} r dr d\varphi \qquad (31)$$

with

$$\varphi(r) = \arccos \frac{r^2+x^2-r_a^2}{2rx}$$

In the above equation $x$ and $\varphi_0$ define the position of the centre of the piston relative to the centre of the tunnel. Equation (31) has been evaluated numerically.

Obviously by using two pistons at $\varphi_0 = \frac{\pi}{4}$ and $\varphi_0 = \frac{3\pi}{4}$ one can ensure that all antisymetric $U_{mn} = 0$ will be zero. Therefore the first mode that can propagate is mode (2,0). If one chooses the position $x$ of the piston so, that $U_{01}$ becomes zero, one can ensure that only higher radial modes can propagate. Therefore we have chosen two inlet tubes in these optimized positions. Thus the developing wave should be quite plane. The main part of the energy of the higher radial modes is concentrated in the tunnel centre. The higher tangential modes have much of their energy centered at $r = 0.5$ and $\varphi = 0$, $\varphi = \pi$. Therefore these modes can be damped easily with small stripes ($30 * 10 * 1000$ mm) made of cellular material placed in the above described regions. With these measures it is possible to get an almost plane wave with a short wave front.

The pressure rising time (the thickness of the wavefront) could be varied by cellular material of different lengths placed along the wall. In the experiments three different values for the thickness of the wavefront $\epsilon$ could be achieved ($\epsilon_0 = 0.605$, $\epsilon_1 = 0.76$, $\epsilon_2 = 0.835$).

# 4 Results

In the following section we will first focus our attention on the theoretical results, that can be derived from section 2 and will then look on the results of the experimental work, that has been undertaken.

## 4.1 Location for pressure measurements, minimum sampling rate

An important result for full–scale or model experiments is, that it is possible (due to the shape of the Eigenfunctions) to give a recommendation for the position of the pressure transducers. If the positions in the cross–section are somewhere along the perimeter then all pressure transducers will give nearly equal signals due to radial waves. So the conclusion would be that the wave is a plane one, though radial waves could exist. Additionally at the perimeter the intensity of a radial wave is less than near the centre. The best position to measure radial waves is the centre of the bottom. At this point the Bessel-functions have their maximum values.

Of course it is not possible to measure any tangential waves at the centre, because their Eigenfunctions are zero in this region. Furthermore if the transducers are located in the region of $\varphi = \frac{\pi}{4}$, $\varphi = \frac{3\pi}{4}$, or $\varphi = \frac{\pi}{2}$ either the symmetric or antisymmetric modes cannot be perceived, because their Eigenfunctions have nodes at this location. If tangential waves are to be detected it is important to distinguish between a single track and a double track tunnel. For a single track tunnel there will exist no antisymmetric tangential waves, because the $U_{mn}$ values of these modes will be zero. The best position would be around $\varphi = \frac{\pi}{2}$. At this location the

Eigenfunctions would be maximal.

In a double track tunnel the $U_{mn}$ values of the symmetric modes will be close to zero. So the best position would be anywhere around $\varphi = \frac{\pi}{4}$ or $\varphi = \frac{3\pi}{4}$.

Of course another possible position for single and double track tunnels would be $\varphi = 0$ and $\varphi = \pi$. But their remains the question whether a ballasted track would lead to substantial distortions in that region. Therefore these positions cannot be recommended.

Due to the fact, that the cross-sectional area of a train is usually (even in double track tunnels) located near the centre of a tunnel, the $U_{mn}$ values for tangential propagating waves will be smaller than for radial waves.

The sampling rate for pressure measurements at the above described points should at least exceed double the value of the cutoff–frequency of the highest mode to be investigated. Due to our experiments the highest mode, that will be perceived, is the third radial mode. For this mode the dimensionless cutoff–frequency is 3.2372. In a tunnel with a diameter of 14 m the cutoff–frequency off the third radial mode is 79.3 Hz. Therefore the sampling rate should be grater than 160 Hz. The first tangential mode that could propagate in such a tunnel has a cutoff-frequency of 14 Hz.

It is not reasonable to measure in more than one point in a cross–section, if these sampling rates cannot be achieved.

## 4.2 Conclusion for the onedimensional theory

For a comparison of the outcomes of numerical calculations with this theory and the model of infinitely thin one-dimensional discontinuities refer to [2].

At the moment let us focus our attention to the region near the discontinuities. For a onedimensional theory we have to use the mean values over the cross–section and from equation (7) and (8) we get

$$\frac{\partial \langle p \rangle}{\partial t} + \frac{\partial \langle w \rangle}{\partial z} = 0 \tag{32}$$

$$\frac{\partial \langle w \rangle}{\partial t} + \frac{\partial \langle p \rangle}{\partial z} = 0 \tag{33}$$

Calculating the average values with the solution (15) and regarding that

$$\iint_S \hat{\Psi}_{mn} dS = 0 \quad m \neq 0 \text{ and } n \neq 0 \tag{34}$$

we find that only the term with $\hat{\Psi}_{00}$ contributes to the solution. The simple one–dimensional linear theory gives a correct result for the mass and the momentum transport. This is valid for the small scale, for the flow in a tunnel on a large scale (z in the range of 100 tunnel diameters) nonlinear effects of the higher mode wave may have a weak influence. However to the knowledge we have gained so far the

tremendous additional effort for the modelling of multidimensional flow on a large scale cannot be justified.

## 4.3 The evaluation method

As an example for the outcome of the experiments and to demonstrate how the number $Mo$ is calculated one experiment is described in this section. The pressure rising time was $\epsilon_0 = 0.605$ and the value of $b = 0.714$. See figure 4 for the experimental setup. The time when the pressure wave coming from the left (see figure 4) arrived at the head of the train was chosen as the starting time for the pressure history. In figure 5 one can see the strong intensities of the higher modes.

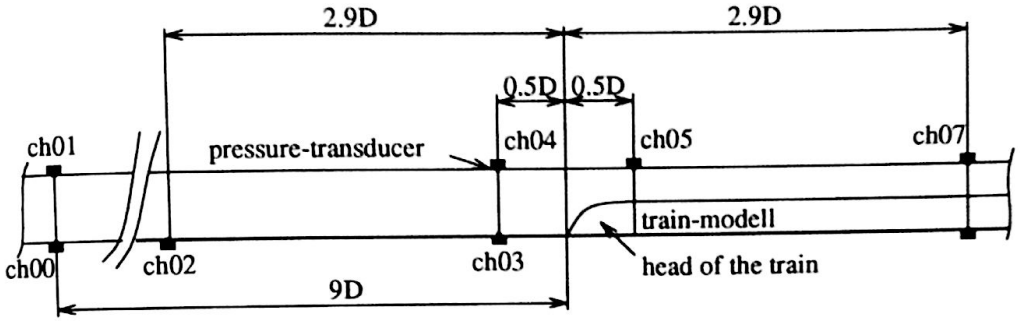


Figure 4: position of pressure transducers

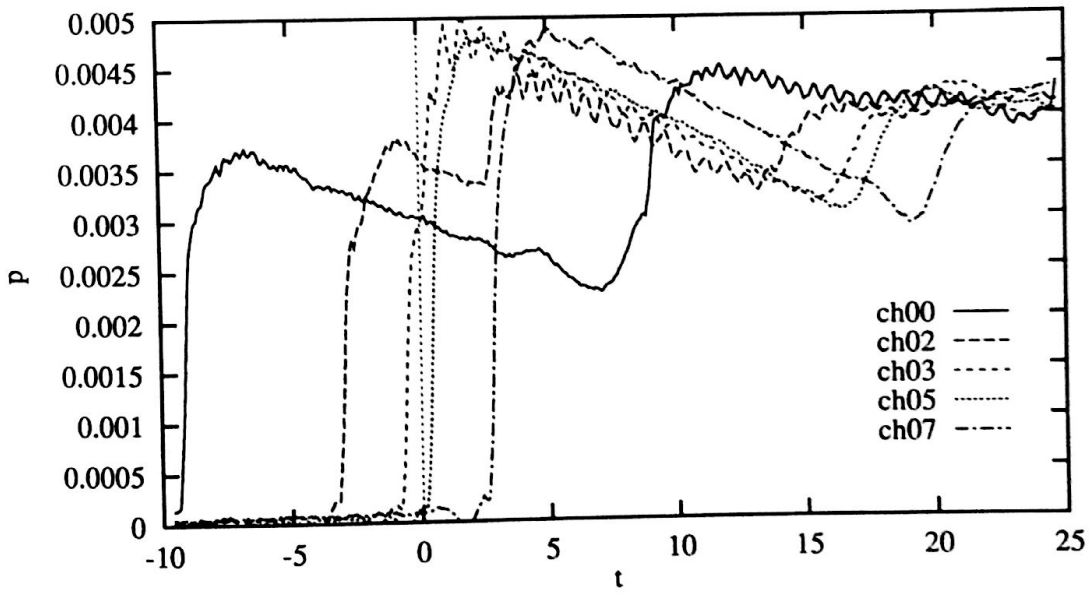


Figure 5: pressure history in the time domain

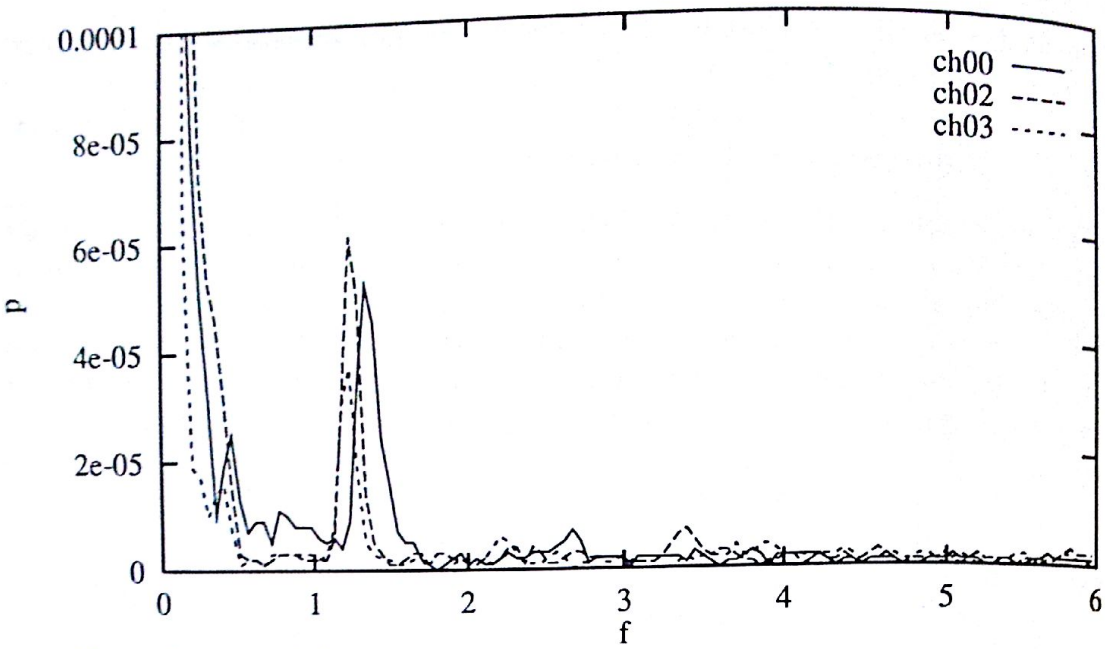


Figure 6: spectral density of pressure signals to the left of the train head

In order to answer the question which modes have been initiated a spectral analysis is made. The window function $w_f$ for each spectral analysis starts shortly after the passing of the wavefront. See table 1 for the beginning ($t_a$), center ($t_m$) and end ($t_e$) of the window function. This long time–window gives of course only a coarse resolution in the transformed time domain, however it allows a fine resolution in the frequency domain.

See figure 6 and 7 for the spectral functions of the signal. Due to the coarse resolution in the time domain, the heights of the peaks give only a rough estimate of the real amplitudes of the higher mode waves. Notice, that the first radial mode is much stronger than the second and third radial mode. The third radial mode can only be seen in CH02. Thus the assumption made in section 2.6, that the pressure should be weighted with the value of $\Lambda_{01}$ for the calculation of the number $Mo$, can be justified.

Notice in figure 7 that almost no higher modes can be perceived in the region of the train. This has also been verified in the numeric simulations (Dissertation by Ottitsch under preparation TU-Wien). The small peak at the dimensionless frequency 2.1 on figure 7 cannot be a higher mode, because its maximum is at the same place at CH05 and CH07, what is in contradiction to the behaviour predicted in section 2.5. This must be a plane modulation of the propagating wave.

Another interesting point is, that the higher mode waves propagate slower than the primary wave. Notice that at CH03 in figure 5 the higher mode waves are located near the front of the reflected wave, but that at the CH00 and CH02 the higher waves are spread out over a much longer time period. Only the high frequency components

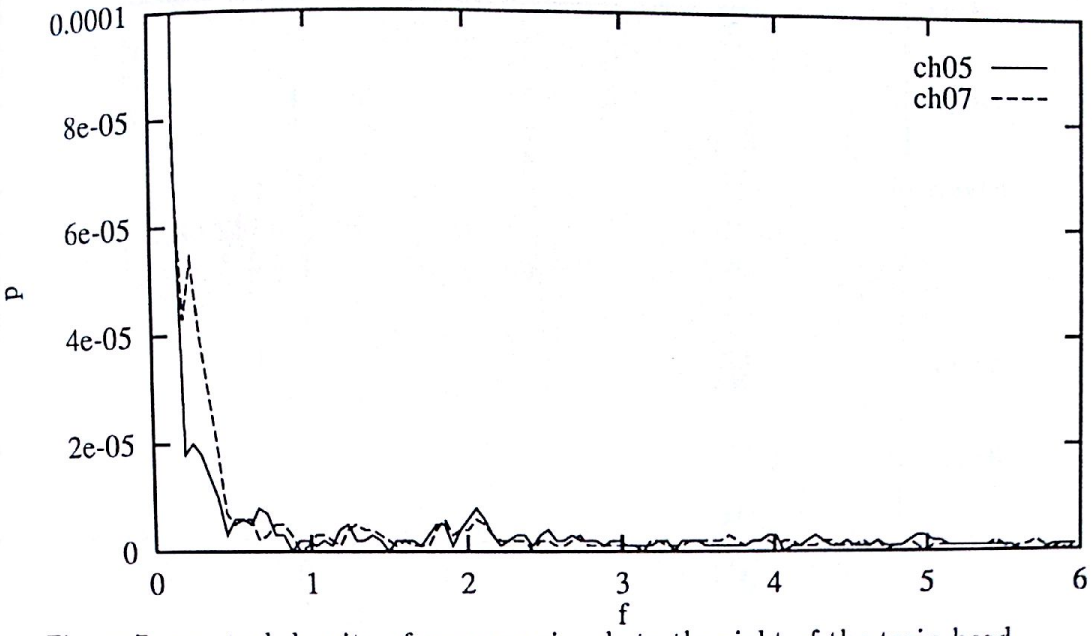


Figure 7: spectral density of pressure signals to the right of the train head

| channel | time–window | | | $f_{mn}^{max}$ theory | | | $f_{mn}^{max}$ experiment | | |
|---|---|---|---|---|---|---|---|---|---|
| | $t_a$ | $t_m$ | $t_e$ | (0,1) | (0,2) | (0,3) | (0,1) | (0,2) | (0,3) |
| ch00 | 1.3 | 11.0 | 20.75 | 1.346 | 2.512 | 3.642 | 1.34 | 2.68 | |
| ch02 | 3.7 | 13.4 | 23.15 | 1.226 | 2.286 | 3.314 | 1.24 | 2.26 | 3.40 |
| ch03 | 9.8 | 19.5 | 29.25 | 1.198 | 2.236 | 3.240 | 1.24 | 2.24 | |
| ch05 | 1.3 | 11.0 | 20.75 | | | | | | |
| ch07 | 3.7 | 13.4 | 23.15 | | | | | | |

Table 1: window for spectral analysis and frequencies of the maxima

of each mode stay near the front of the reflected wave, what can be seen very good at CH00.

In order to measure the height of the higher mode waves the Mo-number has to be calculated. See figure 8 for the filtered signal $p_f$ (described in section 2.6). Notice that the waves near the front of the reflected waves are not higher modes but waves which represent the high frequency components of the wavefront. Therefore this region must not be considered for the evaluation of the Mo-number. The standard deviation of the signal can now be calculated easily. In the next section the *Mo*-number of this and the other experiments is listed.

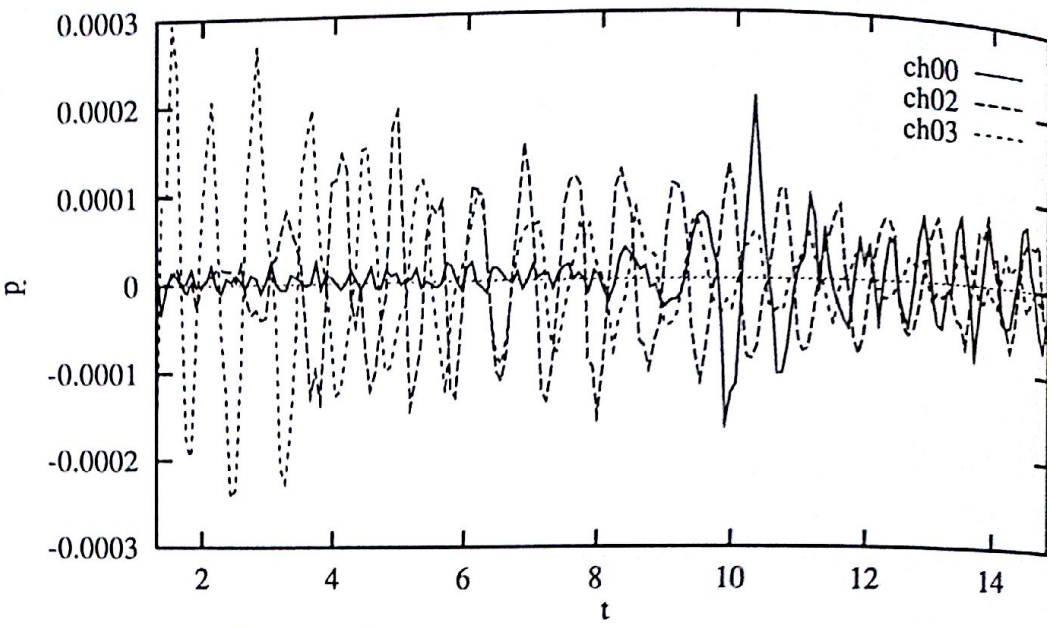


Figure 8: Pressure history of filtered signals

## 4.4 The value of the *Mo*-number in the experiments

As has been shown in the previous sections the value of the number Mo gives a good estimate how strong the higher mode waves are compared to the height of the reflected wave. In this section this value is given in a table for the different configurations (see table 2), that have been investigated. The excentric experiment mentioned in this table was done by placing the centre of the train model cross-section 0.195 diameters from the centre of the tunnel.

| train model type and value of b | $p \approx 0.0035$ | | |
|---|---|---|---|
| | $\epsilon_0$ | $\epsilon_1$ | $\epsilon_2$ |
| without head $b_1 = 0.18$ | * | | |
| without head $b_2 = 0.33$ | * | * | * |
| without head $b_3 = 0.71$ | * | * | * |
| with ICE-like head $b_2 = 0.33$ | * | * | * |
| without head excentric $b_2 = 0.33$ | * | | |
| without head quadratic $b_q = 0.456$ | * | | |

Table 2: Configuration of the different experiments

A simple dimensional analysis shows that the Mo-number depends on the following parameters:

| channel | $t_1$ | $t_2$ | $t_3$ | $t_4$ |
|---|---|---|---|---|
| ch00 | 1.3 | 11.0 | 20.75 | 30.45 |
| ch02 | 3.7 | 13.4 | 23.15 | 32.85 |
| ch03 | 9.8 | 19.5 | 29.25 | 38.95 |

Table 3: Times for the calculation of the Mo-number

| flat head excentric, $b_1 = 0.333$ | | | | | |
|---|---|---|---|---|---|
| $\epsilon$ | $\|z\|$ | $\mathrm{Mo}(t_1,t_2)$ | $\mathrm{Mo}(t_2,t_3)$ | $\mathrm{Mo}(t_3,t_4)$ | $\mathrm{Mo}(t_1,t_4)$ |
| 0.605 | 9 | 0.24 | | | |
| | 2.9 | 0.48 | 0.28 | 0.14 | 0.33 |
| | 0.5 | 0.71 | 0.21 | 0.15 | 0.43 |
| flat head quadratic, $b_q = 0.456$ | | | | | |
| $\epsilon$ | $\|z\|$ | $\mathrm{Mo}(t_1,t_2)$ | $\mathrm{Mo}(t_2,t_3)$ | $\mathrm{Mo}(t_3,t_4)$ | $\mathrm{Mo}(t_1,t_4)$ |
| 0.605 | 9 | 0.30 | | | |
| | 2.9 | 0.58 | 0.23 | 0.13 | 0.37 |
| | 0.5 | 0.71 | 0.12 | 0.07 | 0.42 |

Table 4: Mo-numbers of the train models inside the tunnel

$$Mo = Mo((t_i, t_j), z, b, \epsilon) \tag{35}$$

See table 3 for the different times used for the calculation of the Mo-number.

Since almost no higher mode waves could be perceived in the region where the train was located, the Mo-number has not been evaluated there. On the tables 4 and 5 the values of the Mo-number of the different experiments are given. It is interesting to see, that the value of Mo can exceed 1 for steep waves near the train end. Thus the local pressure fluctuations at such points can be twice as high than the usual plane reflected pressure wave. The value of Mo decreases with the distance from the train head and away from the wave front because the higher mode waves propagate with different group–velocities.

Looking at the values of Mo as a function of the parameter $b$ shows, that the maximum values are neither achieved with very small or very big values of $b$ but somewhere in the middle. Since only three different values of $b$ were investigated, one can only estimate the value of $b$ for a maximum of Mo.

| flat head, $b_1 = 0.181$ | | | | | |
|---|---|---|---|---|---|
| $\epsilon$ | $\lvert z\rvert$ | $\mathrm{Mo}(t_1,t_2)$ | $\mathrm{Mo}(t_2,t_3)$ | $\mathrm{Mo}(t_3,t_4)$ | $\mathrm{Mo}(t_1,t_4)$ |
| 0.605 | 9 | 0.10 | | | |
| | 2.9 | 0.20 | 0.12 | 0.06 | 0.14 |
| | 0.5 | 0.27 | 0.15 | 0.09 | 0.19 |
| flat head, $b_2 = 0.333$ | | | | | |
| $\epsilon$ | $\lvert z\rvert$ | $\mathrm{Mo}(t_1,t_2)$ | $\mathrm{Mo}(t_2,t_3)$ | $\mathrm{Mo}(t_3,t_4)$ | $\mathrm{Mo}(t_1,t_4)$ |
| 0.605 | 9 | 0.54 | | | |
| | 2.9 | 0.96 | 0.40 | 0.18 | 0.61 |
| | 0.5 | 1.07 | 0.20 | 0.16 | 0.64 |
| 0.76 | 9 | 0.35 | | | |
| | 2.9 | 0.72 | 0.25 | 0.12 | 0.45 |
| | 0.5 | 0.85 | 0.15 | 0.13 | 0.50 |
| 0.835 | 9 | 0.13 | | | |
| | 2.9 | 0.29 | 0.12 | 0.08 | 0.19 |
| | 0.5 | 0.40 | 0.13 | 0.04 | 0.24 |
| flat head, $b_3 = 0.714$ | | | | | |
| $\epsilon$ | $\lvert z\rvert$ | $\mathrm{Mo}(t_1,t_2)$ | $\mathrm{Mo}(t_2,t_3)$ | $\mathrm{Mo}(t_3,t_4)$ | $\mathrm{Mo}(t_1,t_4)$ |
| 0.605 | 9 | 0.18 | | | |
| | 2.9 | 0.29 | 0.13 | 0.08 | 0.19 |
| | 0.5 | 0.32 | 0.06 | 0.03 | 0.19 |
| 0.76 | 9 | 0.10 | | | |
| | 2.9 | 0.19 | 0.08 | 0.04 | 0.12 |
| | 0.5 | 0.21 | 0.04 | 0.02 | 0.13 |
| 0.835 | 9 | 0.06 | | | |
| | 2.9 | 0.08 | 0.04 | 0.02 | 0.05 |
| | 0.5 | 0.10 | 0.03 | 0.02 | 0.06 |
| ICE-like head, $b_2 = 0.333$ | | | | | |
| $\epsilon$ | $\lvert z\rvert$ | $\mathrm{Mo}(t_1,t_2)$ | $\mathrm{Mo}(t_2,t_3)$ | $\mathrm{Mo}(t_3,t_4)$ | $\mathrm{Mo}(t_1,t_4)$ |
| 0.605 | 9 | 0.29 | | | |
| | 2.9 | 0.57 | 0.25 | 0.15 | 0.28 |
| | 0.5 | 0.66 | 0.17 | 0.11 | 0.40 |
| 0.76 | 9 | 0.19 | | | |
| | 2.9 | 0.43 | 0.18 | 0.11 | 0.28 |
| | 0.5 | 0.51 | 0.16 | 0.04 | 0.31 |
| 0.835 | 9 | 0.10 | | | |
| | 2.9 | 0.20 | 0.12 | 0.06 | 0.14 |
| | 0.5 | 0.27 | 0.15 | 0.09 | 0.19 |

Table 5: Mo-numbers of the train models inside the tunnel

However a value of $b$ in the range of the blockage ratios of tunnels for high speed trains caused the highest relative pressure fluctuations.

A shape typical for modern highspeed train ends (like the ICE) does reduce such effects.

### Conclusion

Higher mode waves may develop due to the passing of a pressure wave over a train head. The intensities of such waves depend on the pressure rising time of the oncoming wave, the distance from the train head, the distance behind the front of the reflected wave and the ratio between the train and tunnel cross-section. The amplitude of the waves can be of the order of the amplitude of the reflected plane wave.

But these effects happen only in the empty tunnel. These waves cannot be detected in the gap between the train and tunnel walls.

The propagation of these waves can be described with a linear theory showing, that some of the wave phenomenas inside of tunnels can be simulated with linear models.

Regarding the usual theories for one-dimensional flow there is no need to adapt them. If the grid size is chosen smaller than the tunnel diameter the pressure history can be calculated correct (see [2]). However it is not possible to estimate the intensities of the pressure fluctuations due to higher mode waves. An estimate of these values can be taken by interpolations on tables 4 and 5. As these waves do not transport mass or momentum, their existence has no influence on the quality of the results of one-dimensional flow models.

## References

[1] Morse P. M., Ingard K. U.: Theoretical Acoustics 1968 McGraw-Hill Inc.

[2] Ottitsch F., Sockel H., Peiffer A.: The influence of abrupt changes in the cross-sectional area of a railway tunnel on the propagation of pressure waves caused by passing trains. Paper to be published at Proc. 8th Int. Symp. on the Aerodynamics and Ventilation of Vehicle Tunnels Liverpool 1994

[3] Ozawa S. et al.: Countermeasures to reduce micro-pressure waves radiating from exits of shinkansen tunnels. Proc. 7th Int. Symp. on the Aerodynamics and Ventilation of Vehicle Tunnels, pp. 253-266 1991

[4] Peiffer A.: Experimentelle Untersuchungen über mehrdimensionale Druckschwankungen bei Zugfahrten in Eisenbahntunneln. Diplomarbeit TH-Karlsruhe 1994

[5] Pope C. W.: The simulation of flows in railway tunnels using a 1/25 th scale moving model facility, in Haerter A.: Int. Symp. on the Aerodynamics and Ventilation of Vehicle Tunnels, pp. 709-737 Elsevier 1991

[6] Sockel H., Harwarth F.: Unsteady flow due to trains passing a tunnel. Proc. 3rd Int. Symp. on the Aerodynamics and Ventilation of Vehicle Tunnels 1979, pp. 151-160

[7] Sockel H.: Aerodynamik der Schienenfahrzeuge im Tunnel. CCG Lehrgang Schnellbahn-Aerodynamik und Akustik, paper 14 Oberpfaffenhofen 1983

[8] Sockel H., Schultz M.: Strömung bei der Fahrt eines Zuges durch einen kurzen Tunnel, Modellexperimente und Berechnung von Druckverläufen. Final Report for Deutsche Bundesbahn, Wien, April 1990

[9] private correspondence with Wormstall-Reitschuster (Bundesbahn Zentralamt München) from Feb 28, 1992 and Feb 22, 1993 concerning full-scale experiments of the Deutsche Bundesbahn